Results in Physics 8 (2018) 26–33

Contents lists available at ScienceDirect

Results in Physics

journal homepage: www.journals.elsevier.com/results-in-physics

Carbon nanotubes significance in Darcy-Forchheimer flow

Tasawar Hayat [a,b], Kiran Rafique [a], Taseer Muhammad [a,c,*], Ahmed Alsaedi [b], Muhammad Ayub [a]

[a] Department of Mathematics, Quaid-I-Azam University, Islamabad 44000, Pakistan
[b] Nonlinear Analysis and Applied Mathematics (NAAM) Research Group, Department of Mathematics, Faculty of Science, King Abdulaziz University, Jeddah 21589, Saudi Arabia
[c] Department of Mathematics, Government College Women University, Sialkot 51310, Pakistan

ARTICLE INFO

Article history:
Received 29 October 2017
Received in revised form 14 November 2017
Accepted 16 November 2017
Available online 21 November 2017

Keywords:
Darcy-Forchheimer flow
CNTs (SWCNTs and MWCNTs)
Curved stretching surface
Convective boundary condition
Optimal homotopy analysis method (OHAM)

ABSTRACT

The present article examines Darcy-Forchheimer flow of water-based carbon nanotubes. Flow is induced due to a curved stretchable surface. Heat transfer mechanism is analyzed in presence of convective heating process. Xue model of nanofluid is employed to study the characteristics of both single-walled carbon nanotubes (SWCNTs) and multi-walled carbon nanotubes (MWCNTs). Results for both single-walled carbon nanotubes (SWCNTs) and multi-walled carbon nanotubes (MWCNTs) are achieved and compared. Appropriate transformations correspond to strong nonlinear ordinary differential system. Optimal homotopy analysis method (OHAM) is used for the solution development of the resulting system. The contributions of different sundry variables on the velocity and temperature are studied. Further the skin friction coefficient and local Nusselt number are analyzed graphically for both SWCNTs and MWCNTs cases.

Introduction

Nanoparticles through the carbon nanotubes (CNTs) were explored in 1991. Carbon nanotubes (CNTs) are large molecules of pure carbon atoms that are long, thin and cylindrical shaped with diameter ranges $0.7 - 50$ nm. Carbon nanotubes (CNTs) have distinct importance in nanotechnology, optics, conductive plastics, structural composite materials, atomic force microscope, extra strong fibres, demonstration of flat-panel, gas storing, antifouling shade and many others. CNTs are also used as heating source, electrical contacts, resistors and biosensor in medical devices and high temperature refractories. In daily life, CNTs can also acts as antennas for radios and other electromagnetic devices. Carbon nanotubes (CNTs) are categorized as SWCNTs and MWCNTs. Choi et al. [1] developed anomalous enhancement of thermal conductivity in a nanotube suspension. They proved that nanotubes provide largest enhancement of thermal conductivity. Ramasubramaniam et al. [2] studied the homogeneous carbon nanotubes for electrical applications. Xue [3] proposed a model for carbon nanotubes-based composites. Kamali and Binesh [4] analyzed heat transfer enhancement using carbon nanotubes with non-Newtonian nanofluids as a base fluid. Wang et al. [5] illustrated pressure drop and heat transfer of nanofluids in the presence of carbon nanotubes. Haq et al. [6] analyzed squeezing flow of water-based carbon nanotubes between parallel disks. The enhancement of heat transfer in a forward-facing contracting channel using FMWCNT nanofluids is examined by Safaei et al. [7]. Natural convection MHD flow of nanofluid is described by Ellahi et al. [8]. Karimipour et al. [9] analyzed uniform heat flux in forced convection flow of carbon nanotubes in a microchannel. Unsteady squeezing flow of carbon nanotubes with convective surface condition is presented by Hayat et al. [10]. Imtiaz et al. [11] explained flow and heat transfer effects of carbon nanotubes between rotating stretchable disks with thermal radiation and convective condition. Hayat et al. [12] examined Darcy-Forchheimer flow of carbon nanotubes over a rotating disk. Iqbal et al. [13] studied stagnation point flow of carbon nanotubes in the existence of induced magnetic field. Hayat et al. [14] addressed three-dimensional (3D) rotating flow of water-based carbon nanotubes subject to Darcy-Forchheimer porous space. Hayat et al. [15] also discussed combined effects of thermal radiation and melting heat transfer in stagnation-point flow of carbon nanotubes. Ahmed et al. [16] examined thermal radiation and viscous dissipation effects in squeezed flow of carbon nanotubes between Riga plates. Hayat et al. [17] studied homogeneous-heterogeneous reactions effects in three-dimensional flow of water based carbon nanotubes. Haq et al. [18] analyzed thermal performance of engine oil in the presence of both single and multi wall carbon nanotubes between two

* Corresponding author at: Department of Mathematics, Quaid-I-Azam University, Islamabad 44000, Pakistan.
E-mail addresses: taseer_qau@yahoo.com, taseer@math.qau.edu.pk (T. Muhammad).

https://doi.org/10.1016/j.rinp.2017.11.022
2211-3797/

concentric cylinders. Hayat et al. [19] addressed homogeneous-heterogeneous reactions effects in Darcy-Forchheimer flow of carbon nanotubes with different base fluids. Recently Hussain et al. [20] studied three-dimensional flow of carbon nanotubes over a nonlinear stretchable sheet with homogeneous-heterogeneous reactions.

The study of fluid flow through stretching surface has gained wide interest due to its importance and applications in many industrial, technological and engineering problems. Such applications are involved in drawing of plastic films, crystal growing, metal mining, manufacturing and extraction of polymer sheets from dye, cooling of continues filaments, glass blowing, production of paper, manufacturing of meals, sketching of wires, liquid layers in condensation process and several others [21–25]. The simultaneous effects of stretching and heating or cooling during the production process have major impact on the final product. Crane [26] studied the flow due to stretching plate. Crane's work has been extended by many researchers in different directions for both Newtonian and non-Newtonian fluids. Viscous fluid flow due to stretching of curved surface is examined by Sajid et al. [27]. Unsteady flow due to permeable curved shrinking stretching surface is studied by Rosca and Pop [28]. Magnetohydrodynamics (MHD) flow of micropolar fluid due to curved stretchable surface with thermal radiation is reported by Naveed et al. [29]. Abbas et al. [30] analyzed nanofluid flow over curved stretching surface in the presence of slip effects. Hayat et al. [31] investigated magnetohydrodynamic (MHD) flow of due to curved surface with thermal radiation and chemical reaction. Ferrofluid flow due to curved stretching surface with homogeneous-heterogeneous reactions is analyzed by Imtiaz et al. [32]. Recently Hayat et al. [33] also explained MHD flow of micropolar fluid by a curved stretchable surface with homogeneous-heterogeneous reactions.

The convection flows in porous media have wide range of importance and applications in science, industry and environmental systems. Such applications are usually involved in geothermal energy schemes, heat exchanger layouts, modeling of oil reservoir in insulating processes, ground water systems, production of crude oil, nuclear waste disposal, catalytic reactors, fossil fuels beds, units of the energy storage, movement of water in reservoirs and many others. Modified form of classical Darcy model is non-Darcian porous media which incorporates inertia and boundary features. The available literature witnesses that appreciable attention is given to those problems of porous media that are modeled and developed by traditional Darcy's law. The traditional Darcian law is suitable only under the limited range of low velocity and small porosity. This law is incapable for high velocities. Forchheimer [34] added the squared velocity factor in momentum expression to analyze such features. Muskat [35] named this factor as "Forchheimer term". Seddeek [36] investigated viscous dissipation and thermophoresis features in Darcy-Forchheimer mixed convective flow. Analytical solution for non-linear Brinkman-Forchheimer-extended Darcy flow model is provided by Jha and Kaurangini [37]. Hydromagnetic Darcy-Forchheimer flow with variable viscosity is analyzed by Pal and Mondal [38]. Darcy-Forchheimer flow of Maxwell material bounded by convectively heated sheet is examined by Sadiq and Hayat [39]. Shehzad et al. [40] reported Darcy-Forchheimer flow of an Oldroyd-B fluid with Cattaneo-Christov heat flux and nonlinear convection. Forced convection stagnation-point flow towards a shrinking sheet with Darcy-Forchheimer porous medium is analyzed by Bakar et al. [41]. Hayat et al. [42] examined Darcy-Forchheimer flow of Maxwell material with Cattaneo-Christov heat flux and variable thermal conductivity. Umavathi et al. [43] studied the convective flow of nanofluids in a vertical rectangular duct by considering Darcy-Forchheimer-Brinkman model. Muhammad et al. [44] studied Darcy-Forchheimer flow of Maxwell nanofluid with convective boundary condition. Darcy-Forchheimer flow in the presence of Cattaneo-Christov heat flux and homogeneous-heterogeneous reactions is reported by Hayat et al. [45]. Further recent investigations on Darcy-Forchheimer flow can be quoted through the studies [46–50].

The prime objective of present study is to explore the Darcy-Forchheimer flow of water-based carbon nanotubes due to a curved stretchable surface. Heat transfer process is examined by considering convective boundary condition. Optimal homotopy analysis method (OHAM) [51–60] is used to develop the convergent series solutions of velocity and temperature fields. The contributions of different flow variables on velocity and temperature fields are presented and discussed. Skin-friction coefficient and heat transfer rate are also analyzed graphically.

Modeling

Consider steady two-dimensional (2D) flow of water-based carbon nanotubes due to a linear stretchable curved surface coiled in a circle of radius R. Darcy-Forchheimer porous medium and convective boundary condition are also accounted. It is further assumed that the surface is heated through the hot fluid having temperature T_f that gives heat transfer coefficient h_f. We adopt the Curvilinear coordinate system in such a way that s-axis is considered along the linear stretchable curved surface having velocity $u_w(s) = as$ and r-axis is normal to it. The resulting expressions of boundary layer for present flow are

$$\frac{\partial}{\partial r}((r+R)v) + R\frac{\partial u}{\partial s} = 0, \tag{1}$$

$$\frac{u^2}{r+R} = \frac{1}{\rho_{nf}}\frac{\partial p}{\partial r}, \tag{2}$$

$$v\frac{\partial u}{\partial r} + \frac{Ru}{(r+R)}\frac{\partial u}{\partial s} + \frac{uv}{(r+R)} = -\frac{1}{\rho_{nf}}\frac{R}{(r+R)}\frac{\partial p}{\partial s} + \nu_{nf}\left(\frac{\partial^2 u}{\partial r^2} + \frac{1}{(r+R)}\frac{\partial u}{\partial r} - \frac{u}{(r+R)^2}\right) - \frac{\nu_{nf}}{K}u - Fu^2, \tag{3}$$

$$v\frac{\partial T}{\partial r} + \frac{uR}{(r+R)}\frac{\partial T}{\partial s} = \alpha_{nf}\left(\frac{\partial^2 T}{\partial r^2} + \frac{1}{(r+R)}\frac{\partial T}{\partial r}\right), \tag{4}$$

with the boundary conditions

$$u = u_w(s) = as, \quad v = 0, \quad -k_{nf}\frac{\partial T}{\partial r} = h_f(T_f - T) \quad \text{at} \quad r = 0, \tag{5}$$

$$u \to 0, \quad \frac{\partial u}{\partial r} \to 0, \quad T \to T_\infty \quad \text{as} \quad r \to \infty. \tag{6}$$

Here u and v stand for flow velocities in s- and r-directions respectively, ν_{nf} for kinematic viscosity of nanofluid, T for fluid temperature, K for the porous mediums permeability, α_{nf} for thermal diffusivity of nanofluid, $F = \frac{C_b}{sK^{1/2}}$ for non-uniform inertia coefficient of porous medium, C_b for drag coefficient, T_∞ for ambient fluid temperature, p for pressure and a for positive constant. The theoretical model proposed by Xue [3] is given by

$$\mu_{nf} = \frac{\mu_f}{(1-\phi)^{2.5}}, \quad \rho_{nf} = \rho_f(1-\phi) + \rho_{CNT}\phi, \quad \nu_{nf} = \frac{\mu_{nf}}{\rho_{nf}}, \quad \alpha_{nf} = \frac{k_{nf}}{(\rho c_p)_{nf}},$$
$$(\rho c_p)_{nf} = (\rho c_p)_f(1-\phi) + (\rho c_p)_{CNT}\phi, \quad \frac{k_{nf}}{k_f} = \frac{(1-\phi) + 2\phi\frac{k_{CNT}}{k_{CNT}-k_f}\ln\frac{k_{CNT}+k_f}{2k_f}}{(1-\phi) + 2\phi\frac{k_f}{k_{CNT}-k_f}\ln\frac{k_{CNT}+k_f}{2k_f}}, \tag{7}$$

where ϕ stands for volume fraction of nanoparticle, μ_{nf} for nanofluid effective dynamic viscosity, ρ_{nf} for density of nanofluid, $(\rho c_p)_{nf}$ for effective heat capacity of nanofluid, μ_f for dynamic viscosity of base fluid, ρ_{CNT} for carbon nanotubes density, ρ_f for base fluid density, k_{CNT} for thermal conductivity of carbon nanotubes and k_f for base fluid thermal conductivity. Table 1 depicts the thermophysical attributes of water and carbon nanotubes.

Selecting [27,32]:

$$u = asf'(\zeta), \quad v = -\frac{R}{(r+R)}\sqrt{av_f}f(\zeta),$$
$$\zeta = \sqrt{\frac{a}{v_f}}r, \quad \theta(\zeta) = \frac{T-T_\infty}{T_f-T_\infty}, \quad p = \rho_f a^2 s^2 P(\zeta). \tag{8}$$

Continuity Eq. (1) is trivially verified while Eqs. (2)–(8) yield

$$\frac{\partial P}{\partial \zeta} = \left(1-\phi+\phi\frac{\rho_{CNT}}{\rho_f}\right)\frac{f'^2}{(A+\zeta)}, \tag{9}$$

$$\frac{2A}{(A+\zeta)}P = \frac{1}{(1-\phi)^{2.5}}\left(f''' + \frac{f''}{(A+\zeta)} - \frac{f'}{(A+\zeta)^2}\right) + \left(1-\phi+\phi\frac{\rho_{CNT}}{\rho_f}\right)\frac{A}{(A+\zeta)}\left(ff'' - f'^2 + \frac{ff'}{(A+\zeta)}\right) - \frac{\lambda}{(1-\phi)^{2.5}}f' - \left(1-\phi+\phi\frac{\rho_{CNT}}{\rho_f}\right)F_r f'^2, \tag{10}$$

$$\frac{1}{\Pr}\frac{k_{nf}}{k_f}\left(\theta'' + \frac{\theta'}{A+\zeta}\right) + \left(1-\phi+\phi\frac{(\rho c_p)_{CNT}}{(\rho c_p)_f}\right)\frac{A}{(A+\zeta)}f\theta' = 0, \tag{11}$$

$$f(0) = 0, \quad f'(0) = 1, \quad \theta'(0) = -\frac{k_f}{k_{nf}}\gamma(1-\theta(0)), \tag{12}$$

$$f'(\infty) \to 0, \quad f''(\infty) \to 0, \quad \theta(\infty) \to 0. \tag{13}$$

Here A stands for curvature parameter, λ for porosity parameter, F_r for inertia coefficient, Pr for Prandtl number and γ for Biot number. These parameters can be expressed in the following forms:

$$A = R\sqrt{\frac{a}{v_f}}, \quad \lambda = \frac{v_f}{Ka}, \quad F_r = \frac{C_b}{K^{1/2}}, \quad \Pr = \frac{v_f(\rho c_p)_f}{k_f}, \quad \gamma = \frac{h_f}{k_f}\sqrt{\frac{v_f}{a}}. \tag{14}$$

Eliminating pressure P from Eqs. (9) and (10), we get

$$\frac{1}{(1-\phi)^{2.5}\left(1-\phi+\phi\frac{\rho_{CNT}}{\rho_f}\right)}\left((A+\zeta)^3 f^{iv} + 2(A+\zeta)^2 f''' - (A+\zeta)f'' + f'\right) + A\left((A+\zeta)^2 ff''' - (A+\zeta)^2 f'f'' + (A+\zeta)ff'' - (A+\zeta)f'^2 - ff'\right) - \frac{\lambda}{(1-\phi)^{2.5}\left(1-\phi+\phi\frac{\rho_{CNT}}{\rho_f}\right)}\left((A+\zeta)^3 f'' + (A+\zeta)^2 f'\right) - F_r\left((A+\zeta)^2 f'^2 + 2(A+\zeta)^3 f'f''\right) = 0. \tag{15}$$

Table 1
Thermophysical characteristics of CNTs and water [3].

Physical properties	Water	Nanoparticles	
		SWCNTs	MWCNTs
ρ (kg/m^3)	997.1	2600	1600
k (W/mK)	0.613	6600	3000
c_p (J/kg K)	4179	425	796

The non-dimensional forms of coefficient of skin friction and local Nusselt number are

$$\left.\begin{aligned} \mathrm{Re}_s^{1/2}C_f &= \frac{1}{(1-\phi)^{2.5}}\left(f''(0) - \frac{f'(0)}{A}\right), \\ \mathrm{Re}_s^{-1/2}Nu_s &= -\frac{k_{nf}}{k_f}\theta'(0), \end{aligned}\right\} \tag{16}$$

where $\mathrm{Re}_s = u_w s/v_f$ stands for local Reynolds number.

Solutions by OHAM

The optimal series solutions of Eqs. (11) and (15) through the boundary conditions Eqs. (12) and (13) are established by using optimal homotopy analysis method (OHAM). The appropriate linear operators and initial approximations are

$$f_0(\zeta) = e^{-\zeta} - e^{-2\zeta}, \quad \theta_0(\zeta) = e^{-\zeta}, \tag{17}$$

$$\mathcal{L}_f = \frac{d^4 f}{d\zeta^4} - 5\frac{d^2 f}{d\zeta^2} + 4f, \quad \mathcal{L}_\theta = \frac{d^2\theta}{d\zeta^2} - \theta. \tag{18}$$

The above operators satisfy

$$\mathcal{L}_f\left[F_1^* e^{\zeta} + F_2^* e^{-\zeta} + F_3^* e^{2\zeta} + F_4^* e^{-2\zeta}\right] = 0, \quad \mathcal{L}_\theta\left[F_5^* e^{\zeta} + F_6^* e^{-\zeta}\right] = 0, \tag{19}$$

in which F_i^* $(i = 1{-}6)$ depicts the arbitrary constants. The zeroth and mth-order deformation problems can be easily developed in presence of above linear operators. The deformation problems have been computed by using BVPh2.0 of Mathematica.

Convergence analysis

The non-zero auxiliary variables $\hbar_f$ and $\hbar_\theta$ in homotopy solutions regulate the convergence portion and also rate of homotopic solutions. For optimal data of $\hbar_f$ and $\hbar_\theta$, we have used the concept of minimization by considering the average squared residual errors as suggested by Liao [51].

$$\varepsilon_m^f = \frac{1}{k+1}\sum_{j=0}^{k}\left[\mathcal{N}_f\left(\sum_{i=0}^{m}\hat{f}(\zeta)\right)_{\zeta=j\delta\zeta}\right]^2, \tag{20}$$

$$\varepsilon_m^\theta = \frac{1}{k+1}\sum_{j=0}^{k}\left[\mathcal{N}_\theta\left(\sum_{i=0}^{m}\hat{f}(\zeta), \sum_{i=0}^{m}\hat{\theta}(\zeta)\right)_{\zeta=j\delta\zeta}\right]^2. \tag{21}$$

Following Liao [51]:

$$\varepsilon_m^t = \varepsilon_m^f + \varepsilon_m^\theta, \tag{22}$$

where ε_m^t represents total squared residual error, $\delta\zeta = 0.5$ and $k = 20$. At 4th order of approximations, the optimal data of convergence control variables for SWCNTs-Water is $h_f = -0.764361$ and $h_\theta = -0.495141$ and total average squared residual error is $\varepsilon_m^t = 0.0329204$ whereas the optimal data of convergence control variables for MWCNTs-Water is $h_f = -0.69717$ and $h_\theta = -0.529457$ and total average squared residual error is $\varepsilon_m^t = 3.509 \times 10^{-2}$. Figs. 1 and 2 represent the plots of total residual error for SWCNTs-Water and MWCNTs-Water, respectively. Tables 2 and 3 show the individual averaged squared residual errors for SWCNTs-Water and MWCNTs-Water respectively. It is noted that the averaged squared residual errors show decreasing trend for higher order deformations.

Discussion

This portion examines the contributions of different physical parameters like curvature parameter A, nanoparticle volume fraction ϕ, porosity parameter λ, inertial coefficient F_r and Biot number γ on the velocity $f'(\zeta)$ and temperature $\theta(\zeta)$ fields. The results are obtained for both SWCNTs and MWCNTs. Fig. 3 illustrates the impact of curvature parameter A on velocity field $f'(\zeta)$. An increment in curvature parameter A corresponds to higher velocity field $f'(\zeta)$. For larger values of curvature parameter A, the radius of surface enhances which produces an increment in fluid motion. Fig. 4 is plotted to examine that how the velocity profile $f'(\zeta)$ gets affected with the variation of porosity parameter λ. An increment in porosity parameter λ leads to a reduction in the velocity field $f'(\zeta)$. The presence of porous medium increases the resistance to the fluid motion which reduces the fluid velocity and related thickness of momentum layer. Fig. 5 depicts the velocity field $f'(\zeta)$ for varying values of inertia coefficient F_r. Higher values of F_r show decreasing trend for velocity field $f'(\zeta)$. Fig. 6 presents change in velocity field $f'(\zeta)$ for varying values of nanoparticle volume fraction ϕ. For increasing values of nanoparticle volume fraction ϕ, the velocity field $f'(\zeta)$ enhances. Behavior of curvature parameter A on temperature profile $\theta(\zeta)$ is shown in Fig. 7. Larger A yields an enhancement in the temperature field $\theta(\zeta)$. Fig. 8 depicts the change in temperature field $\theta(\zeta)$ for increasing values of porosity parameter λ. Temperature field $\theta(\zeta)$ is enhanced for increasing values of porosity parameter λ. Fig. 9 presents the curves of temperature field $\theta(\zeta)$ for various values of inertia coefficient F_r. Both temperature field $\theta(\zeta)$ and thickness of thermal layer are increasing functions of inertia coefficient F_r. Fig. 10 illustrates the behavior of nanoparticle volume fraction ϕ on temperature field $\theta(\zeta)$. Both temperature field $\theta(\zeta)$ and thermal layer thickness are enhanced for higher nanoparticle volume fraction ϕ. Fig. 11 shows that larger Biot number γ leads to stronger convection which causes an enhancement in temperature $\theta(\zeta)$ and related thickness of thermal layer. Figs. 12 and 13 present the plots of skin friction coefficient $\mathrm{Re}_s^{1/2}C_f$ for varying values of nanoparticle volume fraction ϕ, inertia coefficient F_r and porosity parameter λ. The magnitude of skin friction coefficient $\mathrm{Re}_s^{1/2}C_f$ is enhanced for increasing values of nanoparticle volume fraction ϕ. Figs. 14 and 15 are plotted to analyze the behavior of curvature parameter A, Biot number γ and nanoparticle volume fraction ϕ on local Nusselt number $\mathrm{Re}_s^{-1/2}Nu_s$. Clearly the magnitude of local Nusselt number

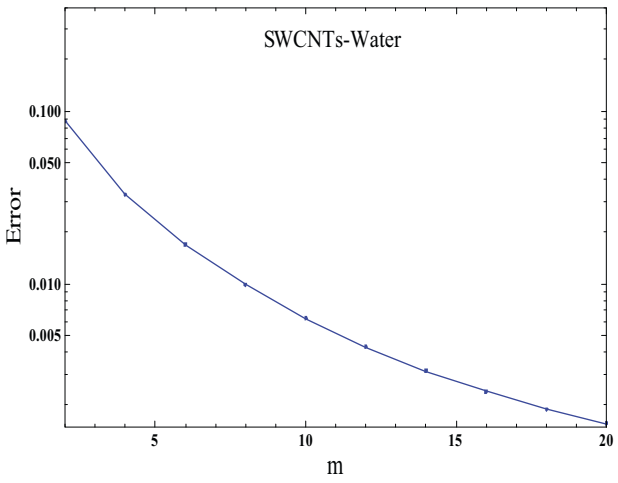

Fig. 1. Total residual error plot for SWCNTs-Water.

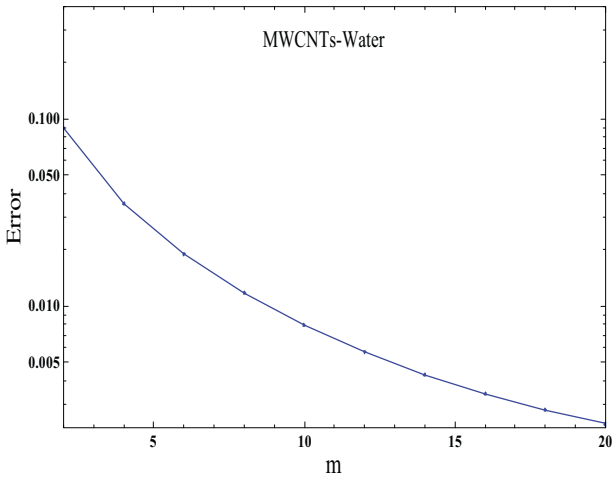

Fig. 2. Total residual error plot for MWCNTs-Water.

Table 2
Individual averaged squared residual errors by considering optimal data of auxiliary variables for SWCNTs-Water.

m	ε_m^f	ε_m^θ
2	6.415×10^{-3}	5.192×10^{-2}
6	2.167×10^{-3}	8.008×10^{-3}
10	1.199×10^{-3}	2.005×10^{-3}
16	6.348×10^{-4}	2.778×10^{-4}
20	4.561×10^{-4}	7.844×10^{-5}

Table 3
Individual averaged squared residual errors by considering optimal data of auxiliary parameters for MWCNTs-Water.

m	ε_m^f	ε_m^θ
2	6.458×10^{-3}	4.589×10^{-2}
6	2.394×10^{-3}	7.190×10^{-3}
10	1.459×10^{-3}	1.748×10^{-3}
16	8.514×10^{-4}	1.949×10^{-4}
20	6.371×10^{-4}	4.837×10^{-5}

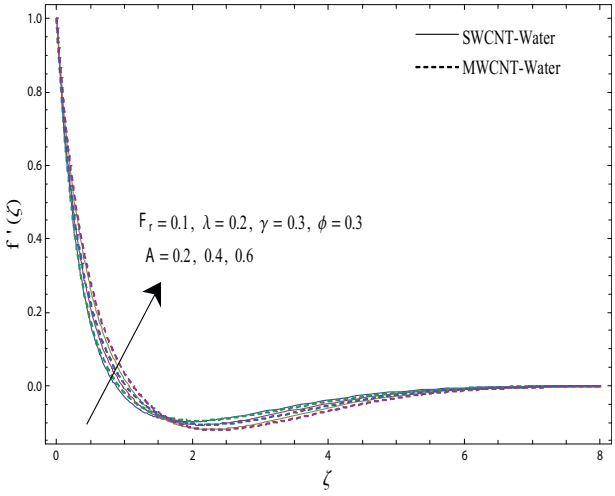

Fig. 3. Plots of $f'(\zeta)$ for A.

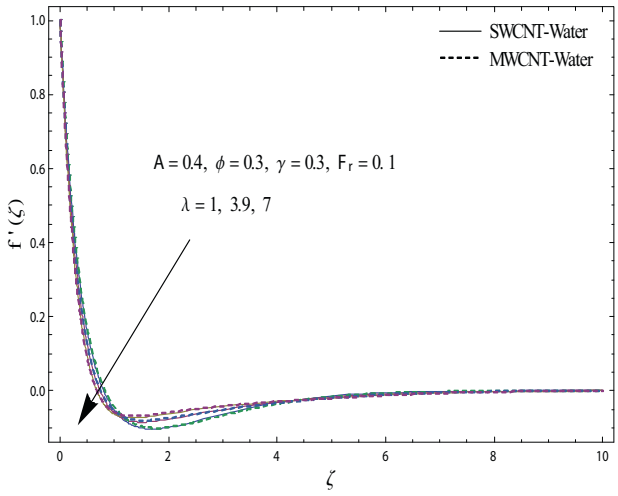

Fig. 4. Plots of $f'(\zeta)$ for λ.

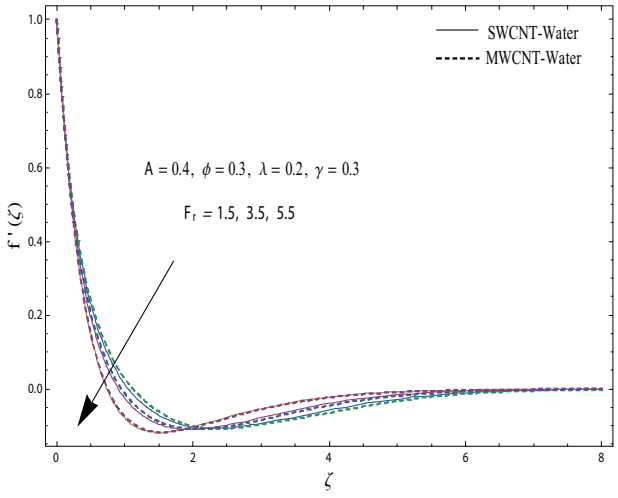

Fig. 5. Plots of $f'(\zeta)$ for F_r.

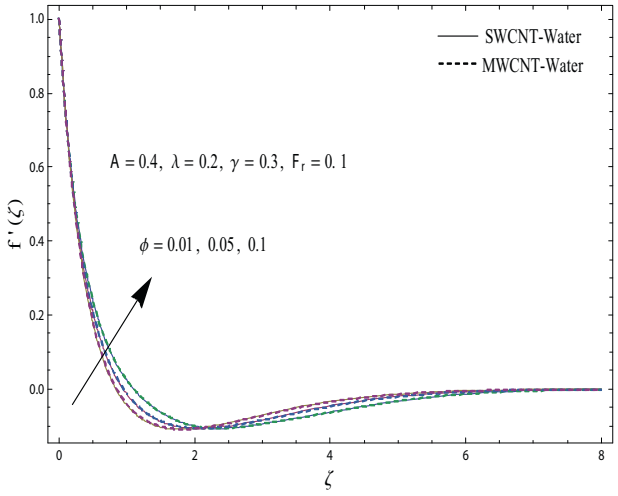

Fig. 6. Plots of $f'(\zeta)$ for ϕ.

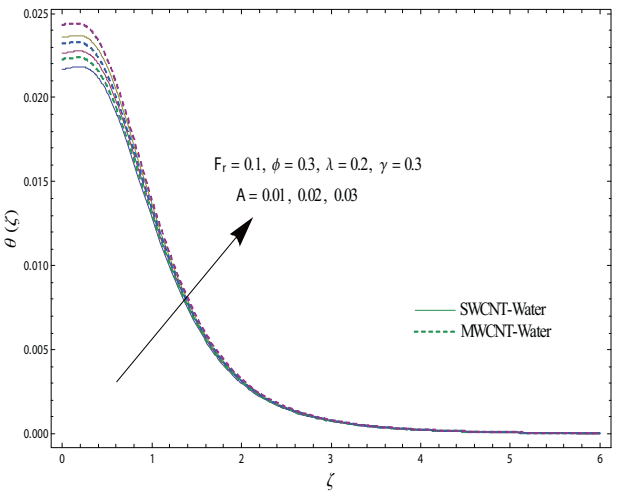

Fig. 7. Plots of $\theta(\zeta)$ for A.

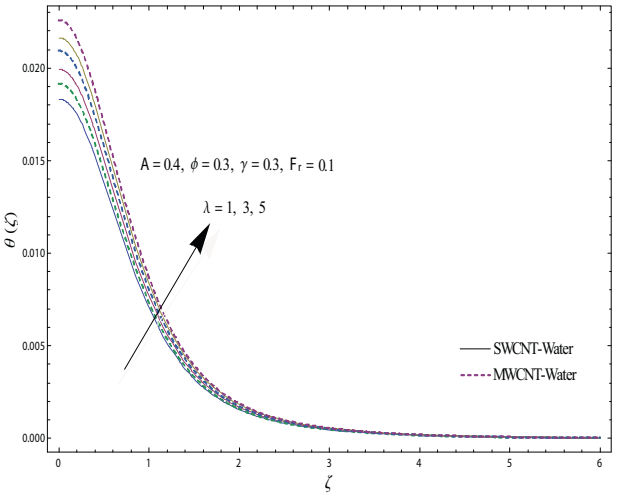

Fig. 8. Plots of $\theta(\zeta)$ for λ.

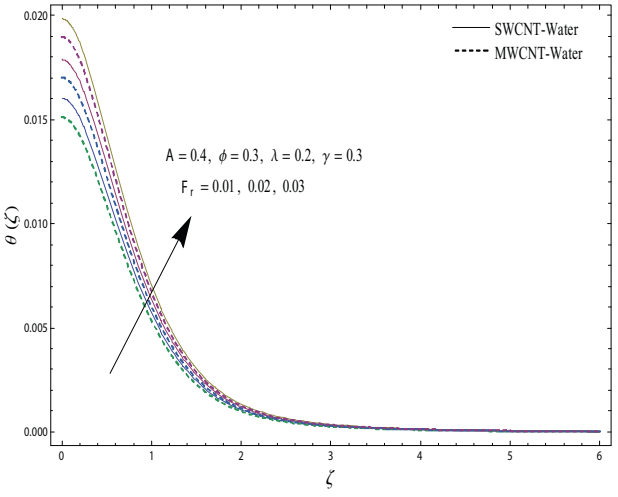

Fig. 9. Plots of $\theta(\zeta)$ for F_r.

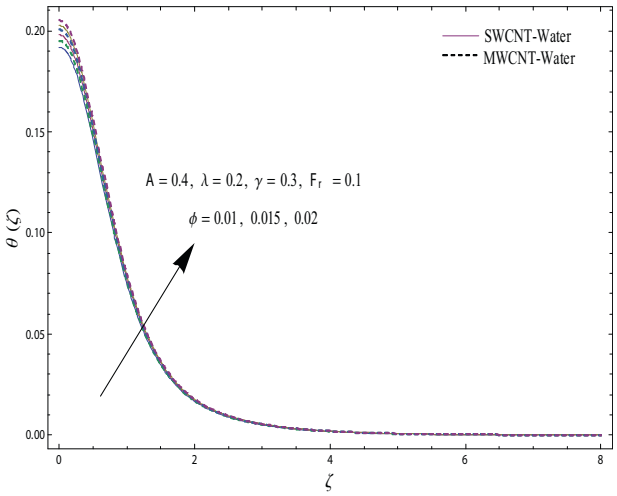

Fig. 10. Plots of $\theta(\zeta)$ for ϕ.

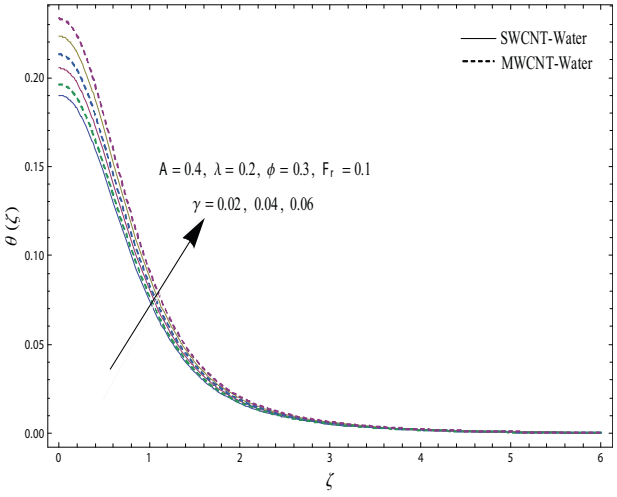

Fig. 11. Plots of $\theta(\zeta)$ for γ.

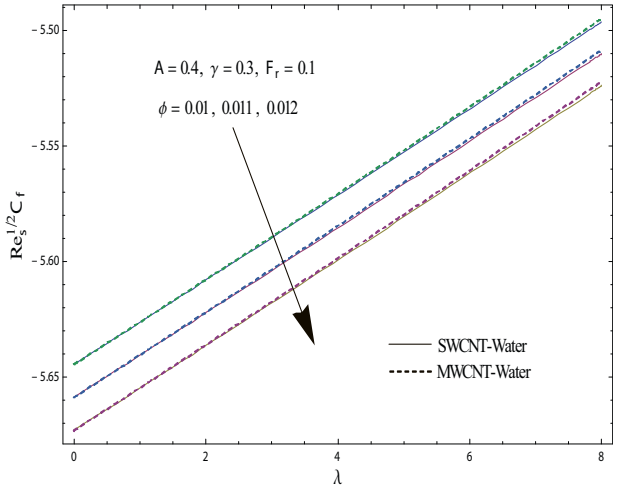

Fig. 12. Plots of $\mathrm{Re}_s^{1/2}C_f$ for ϕ and λ.

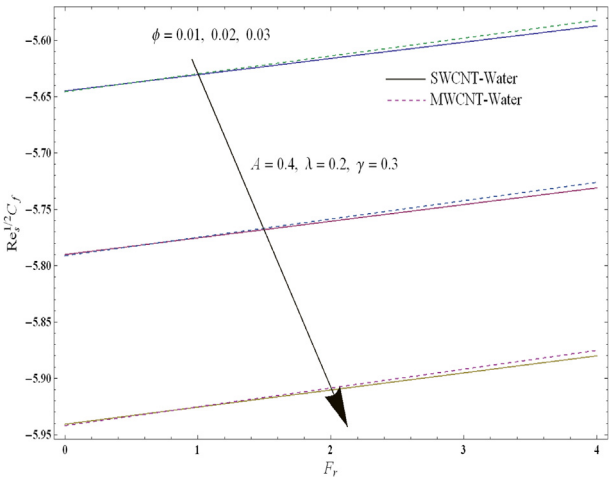

Fig. 13. Plots of $\mathrm{Re}_s^{1/2}C_f$ for ϕ and F_r.

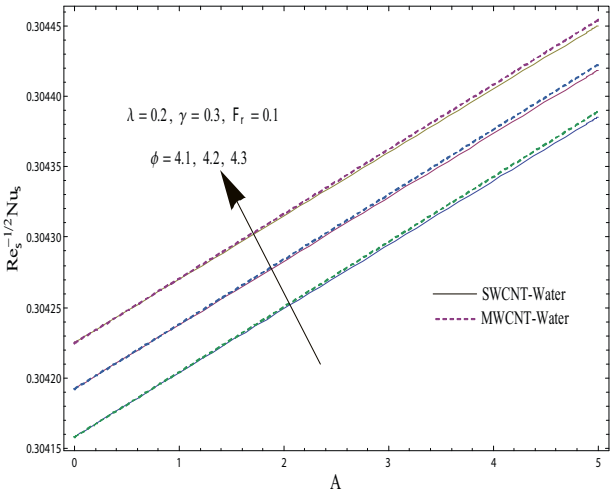

Fig. 14. Plots of $\mathrm{Re}_s^{-1/2}Nu_s$ for ϕ and A.

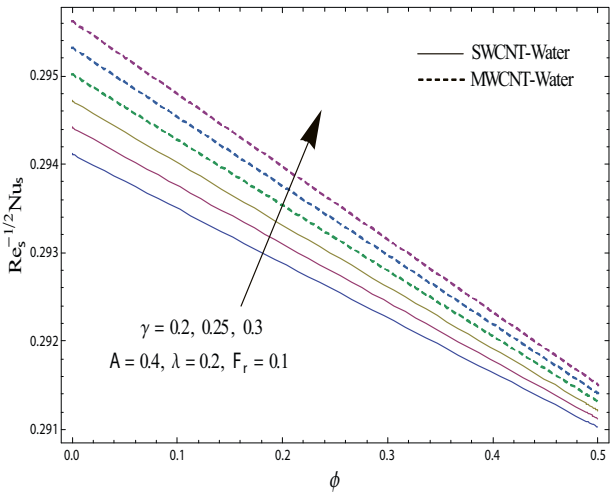

Fig. 15. Plots of $\mathrm{Re}_s^{-1/2}Nu_s$ for ϕ and γ.

$Re_s^{-1/2}Nu_s$ is enhanced for increasing values of nanoparticle volume fraction ϕ and Biot number γ.

Conclusions

Darcy-Forchheimer flow of water-based carbon nanotubes (CNTs) due to convectively heated curved stretching surface is analyzed. Main points are summarized below.

- Both velocity $f'(\zeta)$ and temperature $\theta(\zeta)$ fields are enhanced for larger values of curvature parameter A.
- Larger inertia coefficient F_r and porosity parameter λ show decreasing trend in velocity field $f'(\zeta)$ and momentum layer thickness.
- An increment in nanoparticle volume fraction ϕ leads to higher velocity $f'(\zeta)$ and temperature $\theta(\zeta)$ fields.
- Large Biot number γ has higher temperature field $\theta(\zeta)$ and more thermal layer thickness.
- Skin friction coefficient is enhanced for larger volume fraction of nanoparticle ϕ.
- Heat transfer rate (local Nusselt number) is higher for increasing values of nanoparticle volume fraction ϕ.

References

[1] Choi SUS, Zhang ZG, Yu W, Lockwood FE, Grulke EA. Anomalous thermal conductivity enhancement in nanotube suspensions. Appl Phys Lett 2001;79:2252.
[2] Ramasubramaniam R, Chen J, Liu H. Homogeneous carbon nanotube/polymer composites for electrical applications. Appl Phys Lett 2003;83:2928.
[3] Xue QZ. Model for thermal conductivity of carbon nanotube-based composites. Physica B 2005;368:302–7.
[4] Kamali R, Binesh A. Numerical investigation of heat transfer enhancement using carbon nanotube-based non-Newtonian nanofluids. Int Commun Heat Mass Transfer 2010;37:1153–7.
[5] Wang J, Zhu J, Zhang X, Chen Y. Heat transfer and pressure drop of nanofluids containing carbon nanotubes in laminar flows. Exp Therm Fluid Sci 2013;44:716–21.
[6] Haq RU, Hammouch Z, Khan WA. Water-based squeezing flow in the presence of carbon nanotubes between two parallel disks. Thermal Sci 2014. 148–148.
[7] Safaei MR, Togun H, Vafai K, Kazi SN, Badarudin A. Investigation of heat transfer enhancement in a forward-facing contracting channel using FMWCNT nanofluids. Numer. Heat Transfer, Part A 2014;66:1321–40.
[8] Ellahi R, Hassan M, Zeeshan A. Study of natural convection MHD nanofluid by means of single and multi walled carbon nanotubes suspended in a salt water solutions. IEEE Trans Nanotech 2015;14:726–34.
[9] Karimipour A, Taghipour A, Malvandi A. Developing the laminar MHD forced convection flow of water/FMWNT carbon nanotubes in a microchannel imposed the uniform heat flux. J Magn Magn Mater 2016;419:420–8.
[10] Hayat T, Muhammad K, Farooq M, Alsaedi A. Unsteady squeezing flow of carbon nanotubes with convective boundary conditions. PLoS One 2016;11:e0152923.
[11] Imtiaz M, Hayat T, Alsaedi A, Ahmad B. Convective flow of carbon nanotubes between rotating stretchable disks with thermal radiation effects. Int J Heat Mass Transfer 2016;101:948–57.
[12] Hayat T, Haider F, Muhammad T, Alsaedi A. On Darcy-Forchheimer flow of carbon nanotubes due to a rotating disk. Int J Heat Mass Transfer 2017;112:248–54.
[13] Iqbal Z, Azhar E, Maraj EN. Transport phenomena of carbon nanotubes and bioconvection nanoparticles on stagnation point flow in presence of induced magnetic field. Physica E 2017;91:128–35.
[14] Hayat T, Haider F, Muhammad T, Alsaedi A. Three-dimensional rotating flow of carbon nanotubes with Darcy-Forchheimer porous medium. PLoS One 2017;12:e0179576.
[15] Hayat T, Khan MI, Waqas M, Alsaedi A, Farooq M. Numerical simulation for melting heat transfer and radiation effects in stagnation point flow of carbon-water nanofluid. Comput Methods Appl Mech Eng 2017;315:1011–24.
[16] Ahmed N, Adnan U Khan, Mohyud-Din ST. Influence of thermal radiation and viscous dissipation on squeezed flow of water between Riga plates saturated with carbon nanotubes. Colloids Surf, A 2017;522:389–98.
[17] Hayat T, Ahmed S, Muhammad T, Alsaedi A, Ayub M. Computational modeling for homogeneous-heterogeneous reactions in three-dimensional flow of carbon nanotubes. Results Phys 2017;7:2651–7.
[18] Haq RU, Shahzad F, Al-Mdallal QM. MHD pulsatile flow of engine oil based carbon nanotubes between two concentric cylinders. Results Phys 2017;7:57–68.
[19] Hayat T, Ahmed S, Muhammad T, Alsaedi A. Modern aspects of homogeneous-heterogeneous reactions and variable thickness in nanofluids through carbon nanotubes. Physica E 2017;94:70–7.
[20] Hussain Z, Hayat T, Alsaedi A, Ahmad B. Three-dimensional convective flow of CNTs nanofluids with heat generation/absorption effect: a numerical study. Comput Methods Appl Mech Eng 2018;329:40–54.
[21] Hu Z, Lu W, Thouless MD. Slip and wear at a corner with Coulomb friction and an interfacial strength. Wear 2015;338:242–51.
[22] Hu Z, Lu W, Thouless MD, Barber JR. Simulation of wear evolution using fictitious eigenstrains. Tribology Int 2015;82:191–4.
[23] Hu Z, Thouless MD, Lu W. Effects of gap size and excitation frequency on the vibrational behavior and wear rate of fuel rods. Nucl Eng Des 2016;308:261–8.
[24] Hu Z, Lu W, Thouless MD, Barber JR. Effect of plastic deformation on the evolution of wear and local stress fields in fretting. Int J Solids Struct 2016;82:1–8.
[25] Wang H, Hu Z, Lu W, Thouless MD. The effect of coupled wear and creep during grid-to-rod fretting. Nucl Eng Des 2017;318:163–73.
[26] Crane LJ. Flow past a stretching plate. J Appl Math Phys 1970;21:645–7.
[27] Sajid M, Ali N, Javed T, Abbas Z. Stretching a curved surface in a viscous fluid. Chin Phys Lett 2010;27:024703.
[28] Rosca NC, Pop I. Unsteady boundary layer flow over a permeable curved stretching/shrinking surface. Eur J Mech B Fluids 2015;51:61–7.
[29] Naveed M, Abbas Z, Sajid M. MHD flow of a microploar fluid due to curved stretching surface with thermal radiation. J Appl Fluid Mech 2016;9:131–8.
[30] Abbas Z, Naveed M, Sajid M. Hydromagnetic slip flow of nanofluid over a curved stretching surface with heat generation and thermal radiation. J Mol Liq 2016;215:756–62.
[31] Hayat T, Rashid M, Imtiaz M, Alsaedi A. MHD convective flow due to a curved surface with thermal radiation and chemical reaction. J Mol Liq 2017;225:482–9.
[32] Imtiaz M, Hayat T, Alsaedi A. Convective flow of ferrofluid due to a curved stretching surface with homogeneous-heterogeneous reactions. Powder Technol 2017;310:154–62.
[33] Hayat T, Sajjad R, Ellahi R, Alsaedi A, Muhammad T. Homogeneous-heterogeneous reactions in MHD flow of micropolar fluid by a curved stretching surface. J Mol Liq 2017;240:209–20.
[34] Forchheimer P. Wasserbewegung durch boden. Zeitschrift Ver D Ing 1901;45:1782–8.
[35] Muskat M. The flow of homogeneous fluids through porous media. MI: Edwards; 1946.
[36] Seddeek MA. Influence of viscous dissipation and thermophoresis on Darcy-Forchheimer mixed convection in a fluid saturated porous media. J Colloid Interface Sci 2006;293:137–42.
[37] Jha BK, Kaurangini ML. Approximate analytical solutions for the nonlinear Brinkman-Forchheimer-extended Darcy flow model. Appl Math 2011;2:1432–6.
[38] Pal D, Mondal H. Hydromagnetic convective diffusion of species in Darcy-Forchheimer porous medium with non-uniform heat source/sink and variable viscosity. Int Commun Heat Mass Transfer 2012;39:913–7.
[39] Sadiq MA, Hayat T. Darcy-Forchheimer flow of magneto Maxwell liquid bounded by convectively heated sheet. Results Phys 2016;6:884–90.
[40] Shehzad SA, Abbasi FM, Hayat T, Alsaedi A. Cattaneo-Christov heat flux model for Darcy-Forchheimer flow of an Oldroyd-B fluid with variable conductivity and non-linear convection. J Mol Liq 2016;224:274–8.
[41] Bakar SA, Arifin NM, Nazar R, Ali FM, Pop I. Forced convection boundary layer stagnation-point flow in Darcy-Forchheimer porous medium past a shrinking sheet. Front Heat Mass Transfer 2016;7:38.
[42] Hayat T, Muhammad T, Al-Mezal S, Liao SJ. Darcy-Forchheimer flow with variable thermal conductivity and Cattaneo-Christov heat flux. Int J Numer Methods Heat Fluid Flow 2016;26:2355–69.
[43] Umavathi JC, Ojjela O, Vajravelu K. Numerical analysis of natural convective flow and heat transfer of nanofluids in a vertical rectangular duct using Darcy-Forchheimer-Brinkman model. Int J Thermal Sci 2017;111:511–24.
[44] Muhammad T, Alsaedi A, Shehzad SA, Hayat T. A revised model for Darcy-Forchheimer flow of Maxwell nanofluid subject to convective boundary condition. Chin J Phys 2017;55:963–76.
[45] Hayat T, Haider F, Muhammad T, Alsaedi A. Darcy-Forchheimer flow with Cattaneo-Christov heat flux and homogeneous-heterogeneous reactions. PLoS One 2017;12:e0174938.
[46] Sadiq MA, Waqas M, Hayat T. Importance of Darcy-Forchheimer relation in chemically reactive radiating flow towards convectively heated surface. J Mol Liq 2017;248:1071–7.
[47] Hayat T, Shah F, Alsaedi A, Hussain Z. Outcome of homogeneous and heterogeneous reactions in Darcy-Forchheimer flow with nonlinear thermal radiation and convective condition. Results Phys 2017;7:2497–505.
[48] Hayat T, Haider F, Muhammad T, Alsaedi A. Darcy-Forchheimer flow due to a curved stretching surface with Cattaneo-Christov double diffusion: a numerical study. Results Phys 2017;7:2663–70.
[49] Hayat T, Aziz A, Muhammad T, Alsaedi A. Darcy-Forchheimer three-dimensional flow of Williamson nanofluid over a convectively heated nonlinear stretching surface. Commun Theor Phys 2017;68:387.
[50] Muhammad T, Alsaedi A, Hayat T, Shehzad SA. A revised model for Darcy-Forchheimer three-dimensional flow of nanofluid subject to convective boundary condition. Results Phys 2017;7:2791–7.
[51] Liao SJ. An optimal homotopy-analysis approach for strongly nonlinear differential equations. Commun Nonlinear Sci Numer Simul 2010;15:2003–16.

[52] Dehghan M, Manafian J, Saadatmandi A. Solving nonlinear fractional partial differential equations using the homotopy analysis method. Numer Methods Partial Diff Equ 2010;26:448–79.
[53] Sheikholeslami M, Hatami M, Ganji DD. Micropolar fluid flow and heat transfer in a permeable channel using analytic method. J Mol Liq 2014;194:30–6.
[54] Hayat T, Muhammad T, Alsaedi A, Alhuthali MS. Magnetohydrodynamic three-dimensional flow of viscoelastic nanofluid in the presence of nonlinear thermal radiation. J Magn Magn Mater 2015;385:222–9.
[55] Abd Elmaboud Y, Mekheimer KhS, Mohamed MS. Series solution of a natural convection flow for a Carreau fluid in a vertical channel with peristalsis. J. Hydrodynamics, Ser B 2015;27:969–79.
[56] Turkyilmazoglu M. An effective approach for evaluation of the optimal convergence control parameter in the homotopy analysis method. Filomat 2016;30:1633–50.
[57] Shehzad SA, Hayat T, Alsaedi A, Chen B. A useful model for solar radiation. Energy Ecol Environ 2016;1:30–8.
[58] Hayat T, Ayub T, Muhammad T, Alsaedi A. Flow of variable thermal conductivity Oldroyd-B fluid with generalized Fourier's and Fick's laws. J Mol Liq 2017;234:9–17.
[59] Hayat T, Aziz A, Muhammad T, Alsaedi A. A revised model for Jeffrey nanofluid subject to convective condition and heat generation/absorption. PLoS One 2017;12:e0172518.
[60] Hayat T, Aziz A, Muhammad T, Alsaedi A. Active and passive controls of Jeffrey nanofluid flow over a nonlinear stretching surface. Results Phys 2017;7:4071–8.